Chinese Physics B

PAPER

In-plane uniaxial-strain tuning of superconductivity and charge-density wave in CsV_3Sb_5

To cite this article: Xiaoran Yang *et al* 2023 *Chinese Phys. B* **32** 127101

In-plane uniaxial-strain tuning of superconductivity and charge-density wave in CsV_3Sb_5

Xiaoran Yang(杨晓冉)[1], Qi Tang(唐绮)[1,†], Qiuyun Zhou(周秋韵)[1], Huaiping Wang(王怀平)[1], Yi Li(李意)[1], Xue Fu(付雪)[1], Jiawen Zhang(张加文)[2,3], Yu Song(宋宇)[2], Huiqiu Yuan(袁辉球)[2,3], Pengcheng Dai(戴鹏程)[4], and Xingye Lu(鲁兴业)[1,‡]

[1] *Center for Advanced Quantum Studies and Department of Physics, Beijing Normal University, Beijing* 100875, *China*
[2] *Center for Correlated Matter and School of Physics, Zhejiang University, Hangzhou* 310058, *China*
[3] *State Key Laboratory of Silicon and Advanced Semiconductor Materials, Zhejiang University, Hangzhou* 310058, *China*
[4] *Department of Physics and Astronomy, Rice Center for Quantum Materials, Rice University, Houston, TX* 77005, *USA*

(Received 13 August 2023; revised manuscript received 31 August 2023; accepted manuscript online 6 September 2023)

The kagome superconductor CsV_3Sb_5 with exotic electronic properties has attracted substantial research interest, and the interplay between the superconductivity and the charge-density wave is crucial for understanding its unusual electronic ground state. In this work, we performed resistivity and AC magnetic susceptibility measurements on CsV_3Sb_5 single crystals uniaxially-strained along [100] and [110] directions. We find that the uniaxial-strain tuning effect of T_c ($dT_c/d\varepsilon$) and T_{CDW} ($dT_{CDW}/d\varepsilon$) are almost identical along these distinct high-symmetry directions. These findings suggest the in-plane uniaxial-strain-tuning of T_c and T_{CDW} in CsV_3Sb_5 are dominated by associated c-axis strain, whereas the response to purely in-plane strains is likely small.

Keywords: kagome metal, superconductivity, charge-density wave, uniaxial-strain

PACS: 71.27.+a, 71.45.Lr, 71.10.Pm, 74.25.–q **DOI:** 10.1088/1674-1056/acf707

Materials possessing kagome lattice structures have attracted intense attention due to their unique electronic properties, allowing for the exploration of new and exotic quantum phenomena.[1,2] Among the newly discovered kagome metals, AV_3Sb_5 (A = K, Rb, Cs) exhibits rich quantum phenomena such as non-trivial topological bands, van Hove singularities near the Fermi energy, highly unusual superconductivity, and charge-density waves (CDWs).[3–9] These findings have stimulated a wave of research in this field. Our research focuses on CsV_3Sb_5, a specific member of the AV_3Sb_5 class that has attracted substantial attention for its novel electronic properties.

The structure of CsV_3Sb_5 (space group $P6/mmm$) consists of V–Sb layers intercalated by cesium layers. Within the V–Sb layer, the vanadium cations are coordinated by Sb octahedra, forming a two-dimensional kagome lattice (Fig. 1(a)).[3] CsV_3Sb_5 undergoes a CDW transition at $T_{CDW} \approx 94$ K, and enters into a superconducting ground state at $T_c \approx 3$ K.[4] Various experimental studies revealed long-range CDW order[10–12] and suggested that the unconventional CDW may be related to van Hove filling, in addition to electron–phonon coupling. In addition, electron nematicity has been reported in this system and suggests the CDW to be highly unusual.[13] Despite the relatively low T_c, the superconducting state in CsV_3Sb_5 could be highly unusual. For example, theoretical and transport measurements indicate that charge-4e and charge-6e superconductivity could exist in CsV_3Sb_5.[7,8]

It is well established that the interplay between superconductivity and CDW in CsV_3Sb_5, both of which are related to Fermi surface instability, is essential to understanding the microscopic nature of the electronic ground state. Many experimental techniques, such as elemental substitution (Sn, Nb, Ta),[14–16] mechanical exfoliation,[17,18] hydrostatic pressure,[19–22] uniaxial stress/strain[23,24] have been employed to study the complex interplay between superconductivity and CDW in CsV_3Sb_5. Among these methods, uniaxial strain warrants detailed studies because it is sensitive to symmetry-breaking orders and fluctuations, as well as tuning the physical properties of the system with high precision.

Previously, in-plane uniaxial strain (ε) along the a axis (ε_a) was used to tune the T_c and T_{CDW} in CsV_3Sb_5. The measurements reveal a competition between superconductivity and the CDW. Note that a uniaxial strain applied along the a axis ($\varepsilon_a = \varepsilon_{[110]}$ as $a \parallel [110]$) will induce opposite strains along the other two perpendicular directions (ε_c along the c axis and $\varepsilon_{[\bar{1}10]}$ along the $[\bar{1}10]$ direction, which is equivalent to the [100] direction). Through comparing the results with the tuning of T_c and T_{CDW} by hydrostatic pressure which preserves the D_{6h} symmetry, the authors in Ref. [24] found that the strain-induced ΔT_c and ΔT_{CDW} are driven by the c-axis uniaxial strain (ε_c), while the effect of the symmetry-breaking in-

†Corresponding author. E-mail: qitang@mail.bnu.edu.cn
‡Corresponding author. E-mail: luxy@bnu.edu.cn

plane uniaxial strain is negligible. This is surprising as the in-plane kagome lattice is thought to be essential to the tuning of electronic properties including the superconductivity and the CDW. In addition to the *a*-axis that is parallel with the [110] direction, the [100] direction (30° away from [110]) is another high-symmetry direction, and the response to uniaxial strain along these directions is integral for a comprehensive understanding of the uniaxial-strain-tuning in CsV_3Sb_5.

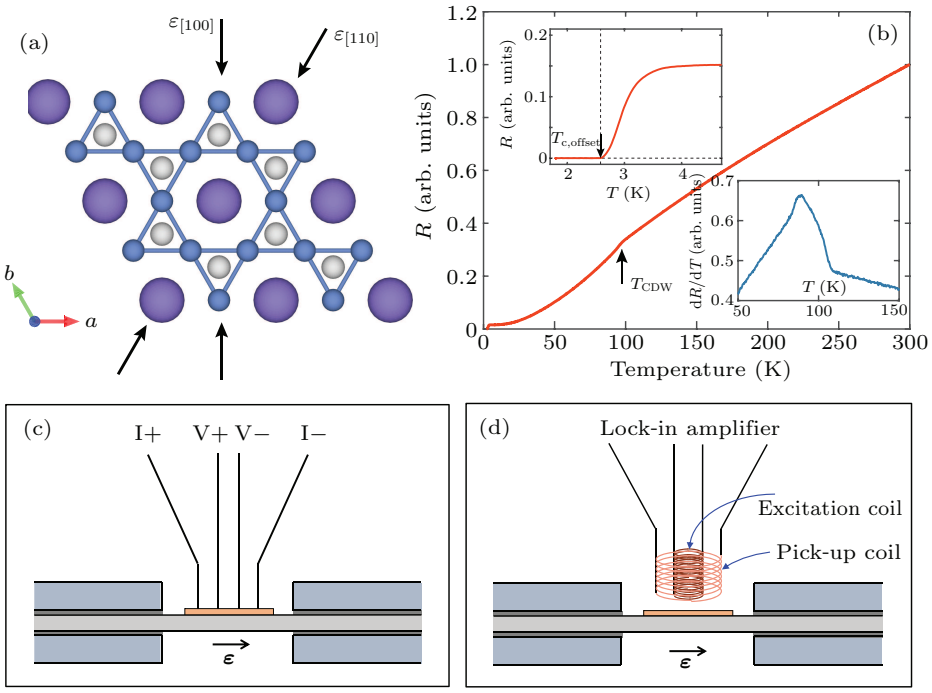

Fig. 1. (a) Top (*c* axis) view of the structure for CsV_3Sb_5. The vanadium ions form an ideal kagome lattice. (b) Temperature-dependent resistivity of CsV_3Sb_5. The left-upper inset shows a zoomed-in view of the superconducting transition at $T_c \approx 3$ K. The vertical arrow marks the $T_{CDW} \approx 94$ K. The right-lower inset shows the zoomed-in view of the first derivative of resistivity dR/dT, in which the peak corresponds to the T_{CDW}. (c)–(d) Schematics of the uniaxial strain application and the measurements of (c) resistivity and (d) AC magnetic susceptibility. Thin (~ 20 μm in thickness) CsV_3Sb_5 single crystal is glued onto a titanium platform (0.1 mm in thickness), which is fixed between the two ends of the sample gap (~ 1 mm). The black thin layers represent the Stycast 2850FT epoxy to help fix the titanium platform. Four silver-paste electrodes are attached to the surface of the crystal in (c) for resistivity measurements. In (d), a commercial MTD100 coil for AC magnetic susceptibility measurement is put over the top of the crystal. The inner coil provides an excitation signal and the outer one collects the signal from the sample. The uniaxial strain is applied by the FC100 strain cell, and the AC susceptibility is measured through an SR830 lock-in amplifier. All the measurements are performed on PPMS.

In this work, we have explored the in-plane uniaxial strain effects on the superconductivity and CDW along the two high-symmetry directions [110] and [100] using the FC100 stress cell (Razorbill Instruments Ltd) which can apply a force up to $F = 90$ N at $T = 4$ K. Our resistivity and AC magnetic susceptibility measurements under uniaxial strains show that the ε-induced ΔT_c and ΔT_{CDW} along the [110] and [100] directions are almost identical. Through decomposing the uniaxial strains into three symmetry channels (ε_{A1g}, ε_{E1g}, and ε_{E2g}) under the D_{6h} point group, we conclude that the in-plane uniaxial strain $\varepsilon_{[110]}$ and $\varepsilon_{[100]}$ show similar and small tuning effects on T_c and T_{CDW}, consistent with the conclusion reported in Ref. [24]. Our results confirmed the dominant role of *c*-axis uniaxial strain in tuning the competing T_c and T_{CDW}, and provide an experimental basis concerning the in-plane uniaxial strain effects on the intertwined orders in CsV_3Sb_5.

The CsV_3Sb_5 single crystals used in this study were grown with the flux method, which was described elsewhere.[3] Our crystals exhibit a superconducting transition at $T_c \approx 3$ K (T_c, offset ≈ 2.6 K) and a CDW transition at $T_{CDW} \approx 94$ K, as shown in Fig. 1(b). The [100] and [110] directions are determined using Laue diffraction, along which the crystals are cut into rectangular bars to facilitate the application of uniaxial strain.

In Ref. [24], the uniaxial strain was applied through a home-built uniaxial-strain apparatus based on piezoelectric stacks. The two ends of a bar-shaped CsV_3Sb_5 single crystal were attached to the two blocks of the apparatus with Stycast 2850FT epoxy.[24] However, given the CsV_3Sb_5 crystals cleave or break easily under uniaxial stress, we use an alternative method developed in the study of the uniaxial-strain effect in FeSe (Ref. [25]). As shown in Figs. 1(c) and 1(d), a thin (~ 20 μm in thickness) CsV_3Sb_5 single crystal is glued onto a ~ 0.1-mm thick titanium platform, which is ~ 10-mm wide at its two ends and has a neck-like part (~ 0.5 mm in width) in the center. The neck of the platform bridges the gap between the two moving blocks of the stress cell. The uniaxial stress is applied to the titanium platform through piezoelectric stacks which drive one of the moving blocks holding one end of the titanium platform. Here, the stress cell has a capacitance to

monitor the force applied to the platform/sample, from which the strain can be determined. Further, the uniaxial strain on the titanium platform can be transferred to the CsV_3Sb_5 thin crystal via a thin layer of epoxy (Stycast 2850FT).

For resistivity measurements, four silver-paste electrodes were made on the surface of the thin CsV_3Sb_5 crystal (Fig. 1(c)), and the longitudinal resistance can be measured by slowly sweeping the temperature under strain and magnetic field. For the measurements of AC magnetic susceptibility, two concentrically nested coils (Razorbill MTD100) placed directly above the sample were used to measure the real part (χ') of the AC magnetic susceptibility (Fig. 1(d)). This signal is provided by a Stanford SR830 lock-in amplifier, which also serves as a reference to extract the signal from the pick-up coil. Due to the received signal's pronounced sensitivity to environmental shifts, the magnetic fluctuations in the sample and its vicinity during the superconductive phase transition, prompted by the Meissner effect, result in a marked variation of the received signal, which allows us to measure the phase transition curve accurately.

Figure 2(a) displays the photos of CsV_3Sb_5 crystals on the FC100 stress cell for the measurements of resistivity (left panel) and AC χ' (right panel). We first measure temperature-dependent resistivity and AC χ' under $\varepsilon_{[110]}$ at low-temperature range to determine the effect on T_c, which had been reported in Ref. [24]. Figures 2(b) and 2(c) show the results of resistivity and AC χ' measured under $\varepsilon_{[110]} = [-0.29\%, 0.29\%]$ and $\varepsilon_{[110]} = [-0.22\%, 0.44\%]$, respectively. To determine the strain-induced changes in T_c, we use the temperatures corresponding to 10% of the resistance at 4 K, and 99.4% of the received signal in the pick-up coil at 4 K, in our resistivity and AC χ' measurements, respectively. Both resistivity and AC χ' reveal that T_c is monotonically tuned with $\varepsilon_{[110]}$. Figure 2(d) plots the ΔT_c as a function of $\varepsilon_{[110]}$ extracted from the data in Figs. 2(b) and 2(c). The ε_a-dependent ΔT_c in Ref. [24] (black squares) is also plotted as a reference. The ΔT_c determined by resistivity and AC χ' results are quantitatively consistent with each other, indicative of the consistency of our experimental methods. Solid lines are fittings of the $\Delta T_c(\varepsilon_{[110]})$ with[24]

$$\Delta T_c(\varepsilon) = a \cdot \varepsilon + b \cdot \varepsilon^2. \tag{1}$$

The fitting parameters a and b are 0.56 and 0.12 in Ref. [24], and 1.27 (1.12) and 0.54 (0.69) in the resistivity (AC χ') measurements, revealing that the linear dependence is dominant, consistent with the results from Ref. [24]. However, the slope $d\Delta T_c/dT$ of our data is much larger than that in Ref. [24]. This could be caused by different ways of determining ΔT_c, a possible overestimate of the uniaxial strain applied on the crystals in Ref. [24], and a slight underestimate of the uniaxial stress applied on the titanium platform in our measurements.

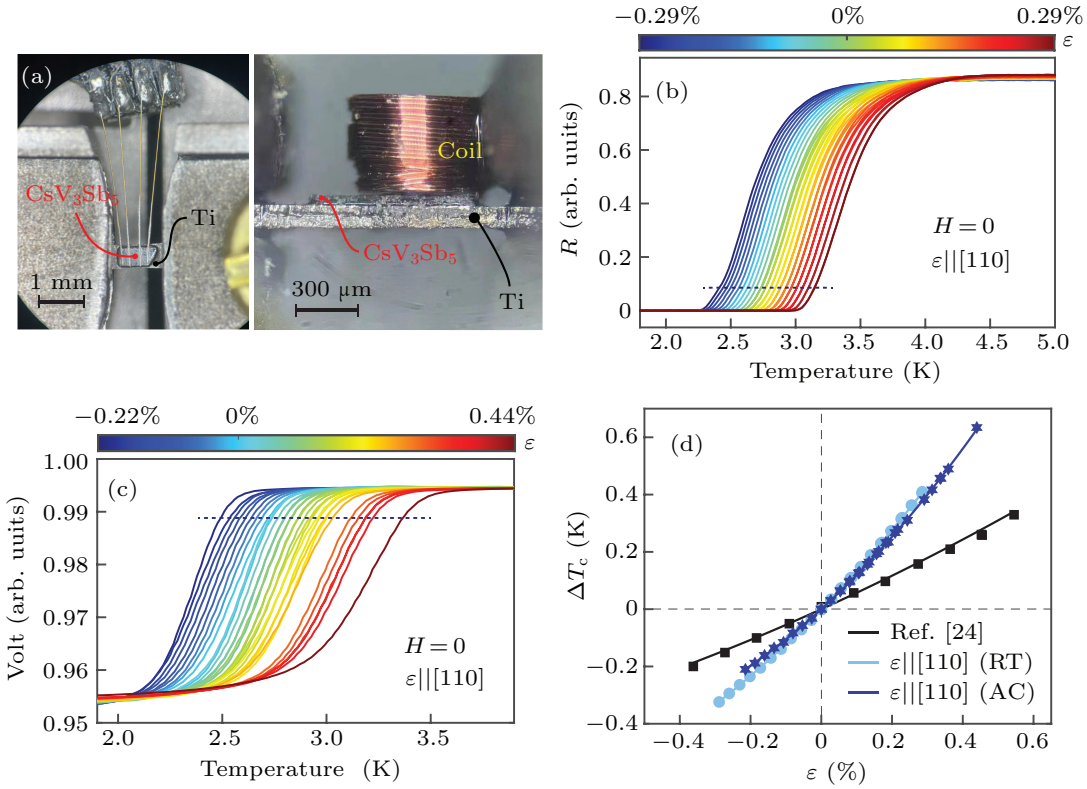

Fig. 2. (a) Photos of the CsV_3Sb_5 single crystals attached on titanium platforms for the measurements of resistivity (left panel) and AC χ' (right panel) under uniaxial strains. (b) Resistivity measurements under the uniaxial strain along the [110] direction, with the strain ε ranging from −0.29% to 0.29%. (c) The measurements of AC χ' under uniaxial strains along the [110] direction with $\varepsilon = [-0.22\%, 0.44\%]$. The horizontal dashed lines mark the values used to track the relative change of T_c. (d) $\varepsilon_{[110]}$ dependence of ΔT_c extracted from the data in panels (b) and (c). The data points labeled by black squares are from Ref. [24]. The solid lines are the fittings of the data with Eq. (1).

Figures 3(a)–3(c) show the resistivity curves under different magnetic fields (H) with $\varepsilon_{[110]} = -0.251\%$, 0%, and 0.285%, respectively. The field dependence of T_c extracted from Figs. 3(a)–3(c) are summarized in Fig. 3(d). By describing the H_{c2} (T) data in Fig. 3(d) using the empirical Ginzburg–Landau equation $H_{c2}(T) = H_{c2}(0)(1-t^2)/(1+t^2)$, the $H_{c2}(0)$ is estimated to be 0.23 T for $\varepsilon_{[110]} = -0.251\%$, 0.30 T for $\varepsilon_{[110]} = 0\%$, and 0.46 T for $\varepsilon_{[110]} = 0.285\%$. Again, the results are consistent with those reported in Ref. [24].

Having presented the ΔT_c ($\varepsilon_{[110]}$), we show in Fig. 4(a) the AC χ' measured under uniaxial strains in the range $\varepsilon_{[100]} = [-0.27\%, 0.27\%]$, through which the $\varepsilon_{[100]}$ dependence of ΔT_c is plotted in Fig. 4(b). The ΔT_c ($\varepsilon_{[110]}$) data shown in Fig. 2(d) are also plotted in Fig. 4(b) for a comparison, revealing that the ΔT_c ($\varepsilon_{[110]}$) and ΔT_c ($\varepsilon_{[100]}$) are almost identical. The fitting of ΔT_c ($\varepsilon_{[100]}$) with Eq. (1) gives $a = 0.97$ and $b = 0.34$, which are close to the fitting parameters of ΔT_c ($\varepsilon_{[110]}$) ($a = 1.12$, $b = 0.69$). The results indicate that $\varepsilon_{[110]}$ and $\varepsilon_{[100]}$ (together with the induced strains along their perpendicular directions) have a similar tuning effect on T_c.

Figures 4(c) and 4(e) are temperature-dependent resistivity curves near T_{CDW} measured under different tensile strains, whose first-order derivatives dR/dT show systematic change with uniaxial strain (Figs. 4(d) and 4(f)). We use the middle value of the slope (rather than the peak position as the peaks are too broad) of dR/dT to characterize the relative change of T_{CDW}. Figure 4(g) summarizes the $\varepsilon_{[100]}$ dependence of ΔT_{CDW} and compares the ΔT_{CDW} ($\varepsilon_{[100]}$) to that reported in Ref. [24] (black squares). The ΔT_{CDW} ($\varepsilon_{[100]}$) is basically the same as ΔT_{CDW} ($\varepsilon_{[110]}$). Taking together the same ΔT_c (ε) along the [110] and the [100] directions, it seems indeed the uniaxial strain applied to these two directions have the same tuning effect on the intertwining orders. These results are consistent with the conclusion in Ref. [24] that a purely in-plane strain has little effect in tunning the competing intertwined orders, and the observed tuning effects of ΔT_c and ΔT_{CDW} result from changes in the c axis induced by the applied in-plane strain, through a nonzero Poisson ratio (ν_{ac}).

To further understand the uniaxial strain effect, we discuss the results from the viewpoint of symmetry. In tetragonal iron pnictides described by the D_{4h} point group, the strain in the A_{1g} channel preserves the symmetry and dictates the ΔT_c (ε_{A1g}) to follow a linear (odd) function, while the strain in antisymmetric B_{1g} and B_{2g} channels require the ΔT_c ($\varepsilon_{B1g/B2g}$) to follow a quadratic (even) function. According to the irreducible representation of the D_{6h} point group associated with the $P6/mmm$ space group, we consider decomposing the strains induced by the uniaxial strains $\varepsilon_{[110]}$ and $\varepsilon_{[100]}$ into the symmetry channels A_{1g}, E_{1g}, and E_{2g} (Fig. 4(h)). Specifically, strains in these channels are $\varepsilon_{A1g,1} = \frac{1}{2}(\varepsilon_{xx}+\varepsilon_{yy})$, $\varepsilon_{A1g,2} = \varepsilon_{zz}$, $\varepsilon_{E1g} = (\varepsilon_{xz}, \varepsilon_{yz})$, and $\varepsilon_{E2g} = \left(\frac{1}{2}(\varepsilon_{xx}-\varepsilon_{yy}), \varepsilon_{xy}\right)$. In this case, the shear strain terms ε_{xz}, ε_{xz}, and ε_{xy}, where x and y respectively correspond to the [110] and [$\bar{1}$10] directions, disappear and we have only ε_{A1g} and $\varepsilon_{E2g} = \frac{1}{2}(\varepsilon_{xx}-\varepsilon_{yy})$ left, which is similar to the case in D_{4h} point group.

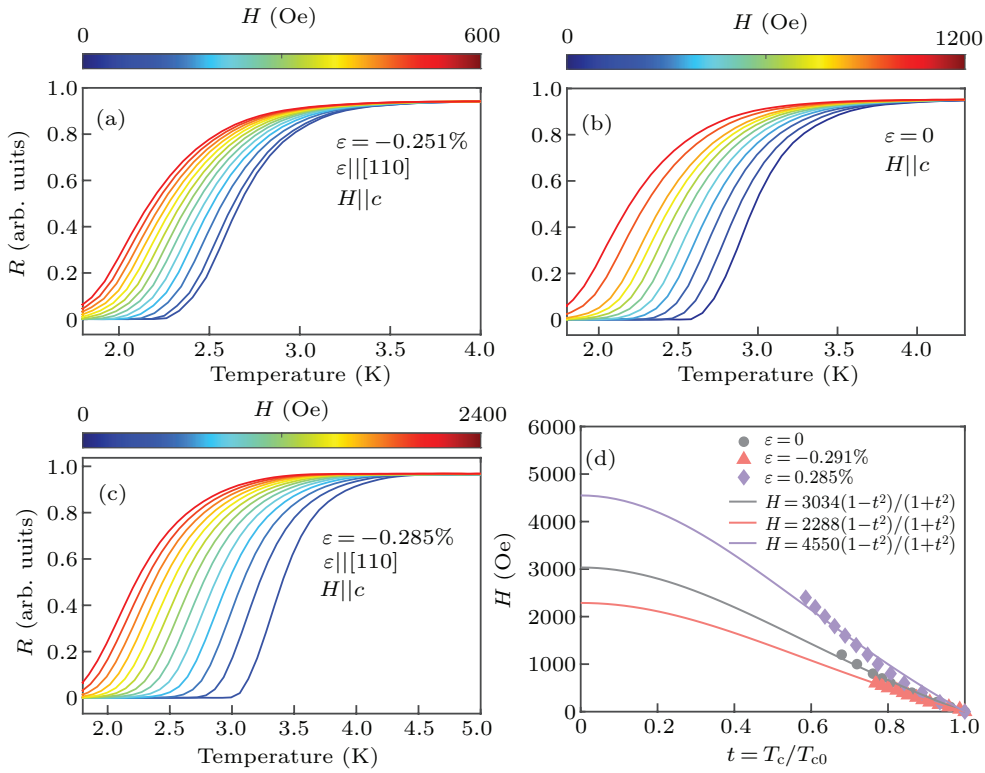

Fig. 3. (a)–(c), Magnetic field dependence of resistivity curves and T_c measured under $\varepsilon = -0.251\%$ (a), $\varepsilon = 0\%$ (b), and $\varepsilon = -0.285\%$ (c). (d) Estimate of H_{c2} for CsV_3Sb_5 under $\varepsilon = -0.251\%$, 0%, and 0.285%. Solid lines are fittings to the Ginzburg–Landau model. The unit 1 Oe = 79.5775 A·m^{-1}.

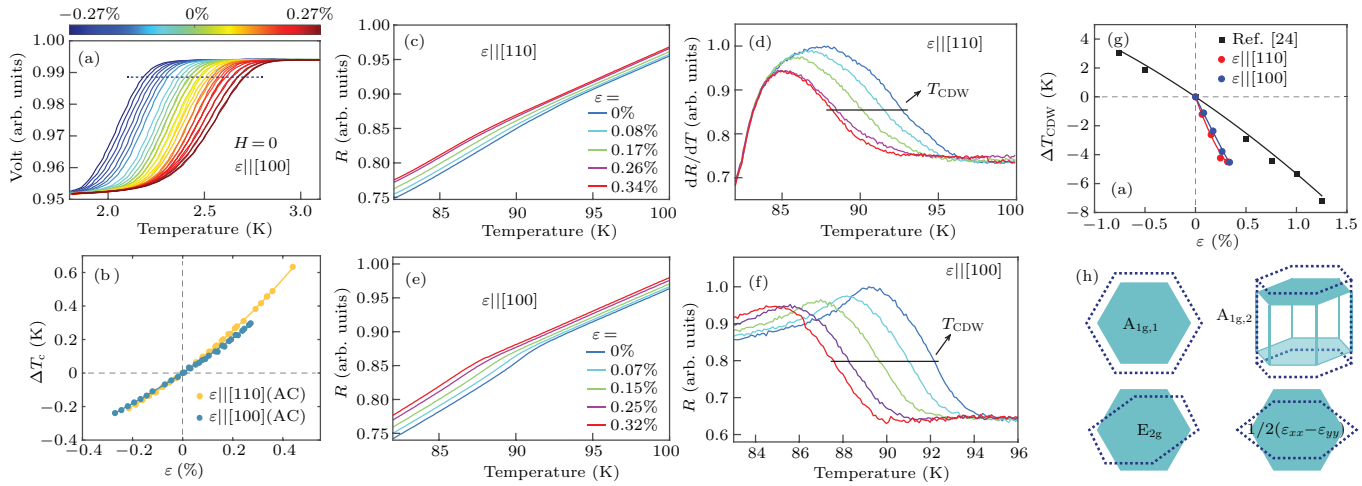

Fig. 4. (a) The results of AC χ' measured under $\varepsilon_{[100]} = [-0.27\%, 0.27\%]$. (b) ΔT_c ($\varepsilon_{[100]}$) extracted from the data in panel (a) (blue dots), and ΔT_c ($\varepsilon_{[110]}$) from Fig. 2(d). The solid lines are the fittings of the data following Eq. (1). (c)–(f) In-plane resistivity measurements under $\varepsilon_{[110]}$ (c) and $\varepsilon_{[100]}$ (e) in the temperature range near T_{CDW}, and (d)–(f) their first-order derivatives dR/dT. The horizontal black lines in panels (d) and (f) mark the values used to determine the T_{CDW} shift. (g) The ε dependence of ΔT_{CDW} for $\varepsilon_{[110]}$ (red dots), $\varepsilon_{[100]}$ (blue dots), and $\varepsilon \parallel [110]$ (black squares) from Ref. [24]. (h) Schematic representation of strains in D_{6h} point group of a hexagonal material.

As the Poisson ratio for the titanium platform holding the crystal is $\nu = 0.32$, $\varepsilon_{[110]}$ will induce $\varepsilon_{[\bar{1}10]} = -\nu\varepsilon_{[110]}$ and $\varepsilon_c = -\nu_{xz}\varepsilon_{[110]}$. Similarly, $\varepsilon_{[\bar{1}10]}$ will induce $\varepsilon_{[110]} = -\nu\varepsilon_{[\bar{1}10]}$ and $\varepsilon_c = -\nu_{yz}\varepsilon_{[\bar{1}10]}$. Thus, the strains induced by $\varepsilon_{[110]}$ (x axis) can be decomposed to symmetric strains $\varepsilon_{A1g,1} = [(1-\nu)/2]\varepsilon_{[110]} = 0.34$, $\varepsilon_{[110]}$ and $\varepsilon_{A1g,2} = -\nu_{xz}\varepsilon_{[110]}$, and $\varepsilon_{E2g} = \frac{1}{2}(\varepsilon_{[110]} - \varepsilon_{[\bar{1}10]}) = 0.66\varepsilon_{[110]}$. The strains induced by $\varepsilon_{[\bar{1}10]}$ (y axis) can be decomposed to $\varepsilon_{A1g,1} = 0.34\varepsilon_{[\bar{1}10]}$, $\varepsilon_{A1g,2} = -\nu_{yz}\varepsilon_{[\bar{1}10]}$, and $\varepsilon_{E2g} = -0.66\varepsilon_{[\bar{1}10]}$. Assuming $\nu_{xz} = \nu_{yz} = \nu'$, $\varepsilon_{[110]}$ and $\varepsilon_{[100]}$ induce the same strain in A_{1g} channel but opposite strain in E_{2g} channel. However, $\varepsilon_{[110]}$ and $\varepsilon_{[100]}$ show almost identical tuning effects on T_c and T_{CDW}, meaning that the in-plane ε_{E2g} strain (in the elastic limit) must have only marginal effect on tuning the intertwining competing T_c and T_{CDW}. Note that our results and analysis cannot distinguish between the role of $\varepsilon_{A1g,1}$ and $\varepsilon_{A1g,2}$, which has been settled by Ref. [24] by comparing their results with the data from hydrostatic pressure.

Our results clarify the effects of in-plane uniaxial strains in tuning the competing orders in CsV_3Sb_5 and corroborate the central conclusion drawn in Ref. [24]. The experimental strategies used in our work can be employed to study a wide class of layered quantum materials possessing intertwined orders.

Acknowledgements

The work at Beijing Normal University is supported by the National Key Projects for Research and Development of China (Grant No. 2021YFA1400400) and the National Natural Science Foundation of China (Grant Nos. 12174029 and 11922402). The work at Zhejiang University was supported by the National Key Research and Development Program of China (Grant No. 2022YFA1402200), the Pioneer and Leading Goose Research and Development Program of Zhejiang Province, China (Grant No. 2022SDX- HDX0005), the Key Research and Development Program of Zhejiang Province, China (Grant No. 2021C01002), and the National Natural Science Foundation of China (Grant No. 12274363). P. D. is supported by the U.S. DOE, BES under Grant No. DE-SC0012311.

References

[1] Yin J X, Lian B and Hasan M Z 2022 *Nature* **612** 647
[2] Neupert T, Denner M M, Yin J X, Thomale R and Hasan M Z 2022 *Nat. Phys.* **13** 137
[3] Ortiz B R, Gomes L C, Morey J R, Winiarski M, Bordelon M, Mangum J S, Oswald I W H, Rodriguez-Rivera J A, Neilson J R, Wilson S D, Ertekin E, McQueen T M and Toberer E S 2019 *Phys. Rev. Mater.* **3** 094407
[4] Ortiz B R, Teicher S M L, Hu Y, Zuo J L, Sarte P M, Schueller E C, Abeykoon A M M, Krogstad M J, Rosenkranz S, Osborn R, Seshadri R, Balents L, He J and Wilson S D 2020 *Phys. Rev. Lett.* **125** 247002
[5] Chapai R, Leroux M, Oliviero V, Vignolles D, Bruyant N, Smylie M P, Chung D Y, Kanatzidis M G, Kwok W K, Mitchell J F and Welp U 2023 *Phys. Rev. Lett.* **130** 126401
[6] Kang M, Fang S, Kim J K, Ortiz B R, Ryu S H, Kim J, Yoo J, Sangiovanni G, Sante D D, Park B G, Jozwiak C, Bostwick A, Rotenberg E, Kaxiras E, Wilson S D, Park J H and Comin R 2022 *Nat. Phys.* **18** 301
[7] Zhou S and Wang Z Q 2022 *Nat. Commun.* **13** 7288
[8] Wang P Y, Xing Y, Yin Q W, Wang A Q, Shen J, Lei H C, Wang Z Q and Wang J 2022 arXiv: 2201.10352
[9] Xu H S, Yan Y J, Yin R T, Xia W, Fang S J, Chen Z Y, Li Y J, Yang W Q, Guo Y F and Feng D L 2021 *Phys. Rev. Lett.* **127** 187004
[10] Broyles C, Graf D, Yang H T, Dong X L, Gao H J and Ran S 2022 *Phys. Rev. Lett.* **129** 157001
[11] Li H, Zhang T T, Yilmaz T, Pai Y Y, Marvinney C E, Said A, Yin Q W, Gong C S, Tu Z J, Vescovo E, Nelson C S, Moore R G, Murakami S, Lei H C, Lee H N, Lawrie B J and Miao H 2021 *Phys. Rev. X* **11** 031050
[12] Liang Z, Hou X, Zhang F, Ma W, Wu P, Zhang Z, Yu F, Ying J J, Jiang K, Shan L, Wang Z and Chen X H 2021 *Phys. Rev. X* **11** 031026
[13] Nie L P, Sun K L, Ma W R, Song D W, Zheng L X, Liang Z W, Wu P, Yu F H, Jian Li J, Shan M, Zhao D, Li S J, Kang B L, Wu Z M, Zhou Y B, Liu K, Xiang Z J, Ying J J, Wang Z Y, Wu T and Chen X H 2022 *Nature* **604** 59
[14] Oey Y M, Ortiz B R, Kaboudvand F, Frassineti J, Garcia E, Cong R, Sanna S, Mitrović V F, Seshadri R and Wilson S D 2022 *Phys. Rev. Mater.* **6** L041801

[15] Li Y K, Li Q, Fan X W, Liu J J, Feng Q, Liu M, Wang C L, Yin J X, Duan J X, Li X, Wang Z W, Wen H H and Yao Y G 2022 *Phys. Rev. B* **105** L180507

[16] Zhong Y G, Liu J J, Wu X X, Guguchia Z, Yin J X, Mine A, Li Y K, Najafzadeh S, Das D, Mielke C, Khasanov R, Luetkens H, Suzuki T, Liu K C, Han X L, Kondo T, Hu J P, Shin S, Wang Z W, Shi X, Yao Y G and Okazaki K 2022 *Nature* **617** 488

[17] Song Y P, Ying T P, Chen X, Han X, Wu X X, Schnyder A P, Huang Y, Guo J G and Chen X L 2021 *Phys. Rev. Lett.* **127** 237001

[18] Song B Q, Ying T P, Wu X X, Xia W, Yin Q W, Zhang Q H, Song Y P, Yang X F, Guo J G, Gu L, Chen X L, Hu J P, Schnyder A P, Lei H C, Guo Y F and Li S Y 2023 *Nat. Commun.* **14** 2492

[19] Chen K Y, Wang N N, Yin Q W, Gu Y H, Jiang K, Tu Z J, Gong C S, Uwatoko Y, Sun J P, Lei H C, Hu J P and Cheng J G 2021 *Phys. Rev. Lett.* **126** 247001

[20] Yu F H, Ma D H, Zhuo W Z, Liu S Q, Wen X K, Lei B, Ying J J and Chen X H 2021 *Nat. Commun.* **12** 3645

[21] Zheng L X, Wu Z M, Yang Y, Nie L P, Shan M, Sun K L, Song D W, Yu F H, Li J, Zhao D, Li S J, Kang B L, Zhou Y B, Liu K, Xiang Z J, Ying J J, Wang Z T, Wu T and Chen X H 2022 *Nature* **611** 682

[22] Yu F H, Zhu X D, Wen X K, Gui Z G, Li Z Y, Han Y L, Wu T, Wang Z Y, Xiang Z J, Qiao Z H, Ying J J and Chen X H 2022 *Phys. Rev. Lett.* **128** 077001

[23] Yin L C, Zhang D T, Chen C F, Ye G, Yu F H, Ortiz B R, Luo S S, Duan W Y, Su H, Ying J J, Wilson S D, Chen X H, Yuan H Q, Song Y and Lu X 2021 *Phys. Rev. B* **104** 174507

[24] Qian T M, Christensen M H, Hu C W, Saha A, Andersen B M, Fernandes R M, Birol T and Ni N 2021 *Phys. Rev. B* **104** 144506

[25] Bartlett J M, Steppke A, Hosoi S, Noad H, Park J, Timm C, Shibauchi T, Mackenzie A P and Hicks C W 2021 *Phys. Rev. X* **11** 021038